Integrated Thin-Film GaSb-based Fabry-Perot Lasers: Towards a Fully Integrated Spectrometer on a SOI Waveguide Circuit

N. Hattasan[1,2], A. Gassenq[1,2], L. Cerutti[3], J.B. Rodriguez[3], E. Tournié[3], G. Roelkens[1,2]

[1] Photonics Research Group-UGent/imec, Sint-Pietersnieuwstraat 41, 9000 Gent, Belgium
[2] Center for nano and biophotonics (NB-Photonics), Ghent University, Belgium
[3]Université Montpellier 2 – CNRS, UMR 5214, Place Bataillon, 34095 Montpellier, France

ABSTRACT

Several molecules of interest have their absorption signature in the mid-infrared. Spectroscopy is commonly used for the detection of these molecules, especially in the short-wave infrared (SWIR) region due to the low water absorption. Conventional spectroscopic systems consist of a broadband source, detector and dispersive components, making them bulky and difficult to handle. Such systems cannot be used in applications where small footprint and low power consumption is critical, such as portable gas sensors and implantable blood glucose monitors. Silicon-On-Insulator (SOI) offers a compact, low-cost photonic integrated circuit platform realized using CMOS fabrication technology. On the other hand, the GaSb material system allows the realization of high performance SWIR lasers and detectors. Integration of GaSb active components on SOI could therefore result in a compact and low power consumption integrated spectroscopic system.

In this paper, we report the study on thin-film GaSb Fabry-Perot lasers integrated on a carrier substrate. The integration is achieved by using an adhesive polymer (DVS-BCB) as the bonding agent. The lasers operate at room temperature at 2.02µm. We obtain a minimum threshold current of 48.9mA in the continuous wave regime and 27.7mA in pulsed regime. This yields a threshold current density of 680A/cm^2 and 385A/cm^2, respectively. The thermal behaviour of the device is also studied. The lasers operate up to 35 °C, due to a 323 K/W thermal resistance

Keywords: SOI photonic integrated circuit, GaSb lasers, BCB bonding, short-wave infrared, integrated laser

1. INTRODUCTION

Shortwave-infrared spectroscopy (2-3 µm wavelength range) is particularly interesting for several applications such as gas analysis [1], trace gas detection [2] and glucose concentration monitoring [3]. The combination band of vibrational-rotational states of several interesting gases such as CO, CO_2, CH_4 are located in this wavelength region, while the interference of water absorption is relatively low.

Over the past few years, sources and detectors have been developed for these applications. GaSb-based semiconductors have emerged as very promising materials which provide high performance, compact, single mode lasers operating at room temperature with high output power[4][5]. On the other hand, Silicon-On-Insulator (SOI) allows realizing highly compact integrated optical circuits [6], using a fabrication process that is CMOS compatible [7]. Therefore, it allows high volume manufacturing with low cost. Moreover, SOI waveguide circuits are transparent in the short-wave infrared [8], enabling the realization of the envisioned short-wave infrared photonic integrated circuits.

Although SOI is a suitable platform for shortwave infrared photonic integrated circuits, it is not possible to be processed into lasers and detectors due to its indirect band gap. Therefore, the heterogeneous integration of SOI and GaSb-based compounds is highly desirable. Several works have been reported on the integration of GaSb-based detectors on SOI with good performance [9-10]. There are to our knowledge no reports on the integration of GaSb-based lasers on SOI, although, several demonstrations on the InP/SOI heterogeneous integration platform have been reported [11][12].

In this paper, we report, for the first time, the heterogeneous integration of GaSb-based Fabry-Perot lasers onto a carrier substrate, as a stepping stone towards the full integration on a SOI waveguide circuit. We will describe the GaSb epitaxy design, the laser fabrication process and the measurement results.

Updated 1 March 2012

2. EPITAXY DESIGN

The epitaxy is grown by conventional solid source molecular beam epitaxy (MBE) on an n-type GaSb substrate. The heterostructure consists of 300 nm Be-doped GaSb ($1x10^{19}$ cm^{-3}) as p-contact and 300 nm Te-doped GaSb ($2x10^{18}$ cm^{-3}) as n-contact. A 1 µm thick $Al_{0.9}Ga_{0.1}As_{0.07}Sb_{0.93}$ cladding layer is used on both sides of the active region ($2x10^{18}$ cm^{-3} Be/Te doping respectively). Composition grading is performed between the contact and cladding layer over 100nm thickness. 360 nm thick $Al_{0.25}Ga_{0.75}As_{0.02}Sb_{0.98}$ separate confinement layers (SCH) are used. The active region is made of four 10 nm $In_{0.24}Ga_{0.76}As_{0.01}Sb_{0.99}$ quantum wells separated by three 30nm thick $Al_{0.25}Ga_{0.75}As_{0.02}Sb_{0.98}$ barriers. InAsSb is used between the GaSb substrate and the GaSb contact layer as etch stop layer for the bonding process. Figure 1(a) represents the band diagram of the epitaxy. The stack is designed to have its peak emission at 2.05 µm. Figure 1(b) represents its refractive index profile and fundamental optical mode profile. The confinement factor in the QWs and in the p-cladding layer is 7.4% and 2.9% respectively. The simulated modal loss is 1.4 cm^{-1}. The simulation is carried out using a full-vectorial 2D eigenmode expansion method [13].

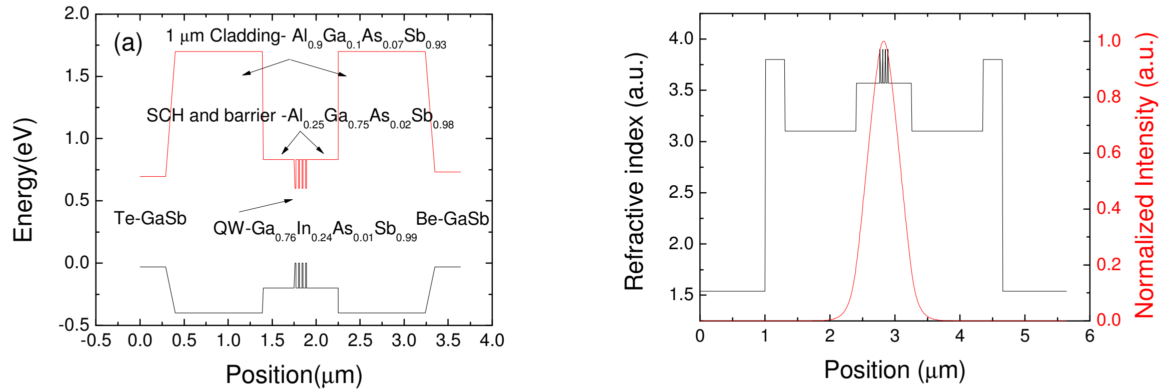

Figure 1: (a) Energy band diagram of the laser epitaxy (b) Fundamental optical mode profile

3. FABRICATION

The fabrication of the thin-film laser can be divided into 2 parts: (a) the integration of the epitaxial material onto the carrier wafer and (b) the laser fabrication.

3.1 Integration technology

Prior to the integration process, the epitaxial die and carrier wafer is cleaned using Acetone and Isopropanol. An InP wafer is chosen as carrier wafer in this experiment in order to allow for easy cleaving of the Fabry-Perot lasers. The carrier wafer is dehydrated using a bake at 150 ºC. Benzocyclobutene (DVS-BCB) is then spin coated on the carrier wafer. The thickness of the DVS-BCB layer can be adjusted by diluting the commercially available solutions with mesitylene. After spin coating, the carrier is baked at 150 ºC for 3 minutes to remove the mesitylene. The epitaxial die is then transferred onto the carrier wafer. The sample is then baked at 250 ºC for 1 hr to cure the DVS-BCB. The GaSb growth substrate is mechanical grinded down to approximately 50 µm thickness. Wet etching (CrO_3:HF:H_2O 1:1:3 v/v) is used to remove the rest of the substrate. Figure 2(a) shows the epitaxial film on the carrier after the substrate removal process. With this process, it is possible to achieve bonding thicknesses down to 50nm. A scanning electron microscope (SEM) image of the bonding interface is shown in figure 2(b).

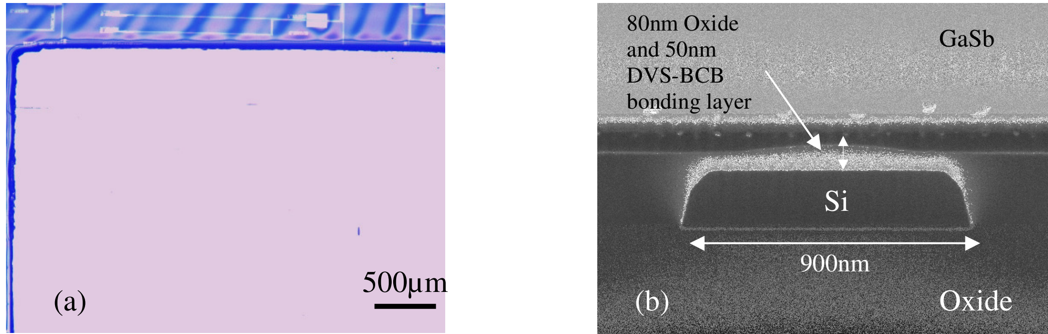

Figure 2: (a) optical image of the bonded device; (b) SEM image of the bonding interface

3.2 Laser fabrication

After substrate removal, the etch stop layer (InAsSb) is removed by wet etching (citric acid:H_2O_2 2:1 v/v). The p-contact metallization (Ti/Pt/Au 2/35/100nm) is then deposited using electron beam evaporation. The laser mesa is formed by wet etching using two lithography steps. Firstly, the GaSb p-contact is etched using a citric acid:H_2O_2:H_3PO_4:H_2O mixture (55:5:3:220 v/v). The $Al_{0.9}Ga_{0.1}As_{0.07}Sb_{0.93}$ cladding is then etched using a HCl-based mixture (HCl:H_2O:H_2O_2 50:100:1 v/v). After a 2nd lithography, which is required to protect the etched mesa, the QWs and SCH region are then etched using the citric acid:H_2O_2:H_3PO_4:H_2O mixture. The n-cladding is then again removed using the HCl-based mixture. AuGe/Ni/Au(150/60/100nm) is deposited as n-contact using a thermal evaporator system. DVS-BCB (3022-46) is used to planarize and passivate the laser. Reactive ion etching (RIE) is used to etch the DVS-BCB for contact via opening. 50/500nm Ti/Au is then deposited for probing. Before cleaving the sample, the carrier is grinded down to approximately 200µm in order to accommodate the cleaving process such that good facet is obtained. Figure 3 presents a summary of the laser fabrication process. Figure 4(a) shows a top view optical image of the laser and figure 4(b) presents a SEM image of the facet and the cross section of the realized device. A DVS-BCB bonding layer thickness of 730 nm is used in these experiments.

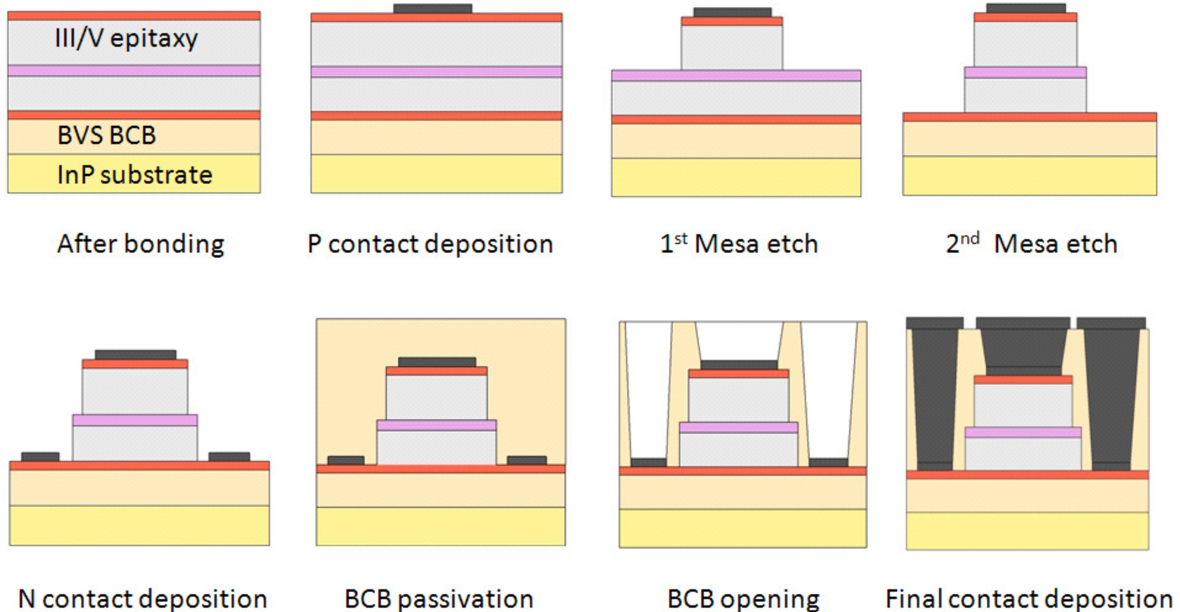

Figure 3: process flow of the laser fabrication process

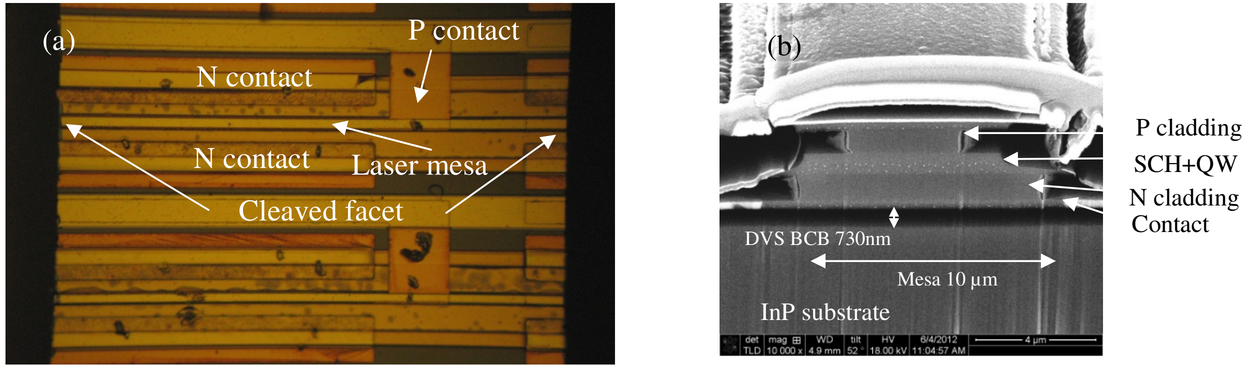

Figure 4: (a) optical image of the cleaved laser bar (b) SEM image of one of the laser cross sections

4. MEASUREMENT RESULTS

The measurement set up consists of a Keithley 2400 for continuous wave (CW) current injection and a Lightwave LDP-3811 current source for pulsed measurements. A Yokogawa optical spectrum analyzer is used for spectral analysis. Light is collected using multimode fiber with a fiber diameter core of 50 µm. A thermo-electric cooler is used to control the temperature of the substrate. Laser characteristic has been measured and studied in 3 aspects: LIV curves and the associated optical spectra, the thermal characteristics and the specific contact resistance.

4.1 LIV characteristics and laser spectrum

The measurement of the LIV curves is conducted at room temperature without temperature controller. The LIV characteristic of a typical laser is presented in figure 5(a). The laser mesa is 15 µm wide and 490 µm long. The threshold current is 31mA in pulsed regime and 49.7mA in CW regime corresponding to a current density of 422 and 676 A/cm^2 respectively. The maximum output power of this component is 58µW at 77mA. The series resistance is 14.3 Ohm. Laser spectra at different bias current are shown in figure 5(b). As we can see, the peak wavelength shifts towards longer wavelength with the increase of bias current due to self-heating.

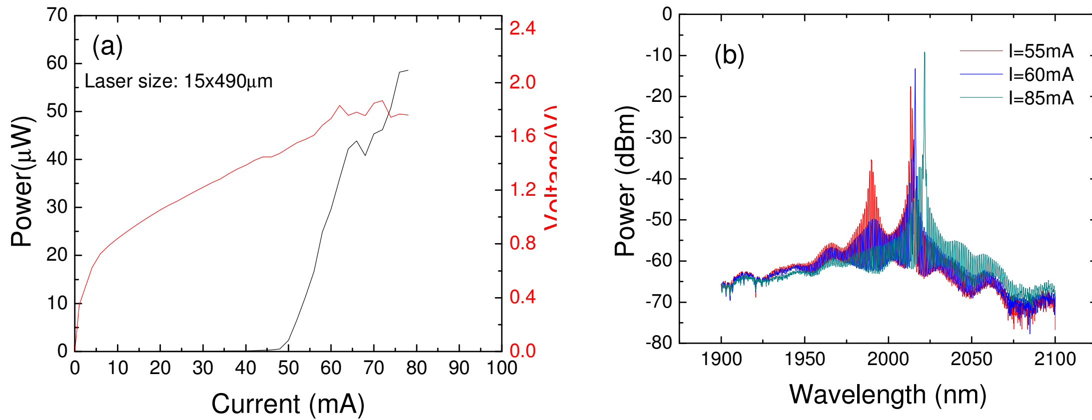

Figure 5: (a) FP laser characteristic (490 µm x 15 µm device dimensions): (a) LIV characteristic (b) laser spectrum at different bias current

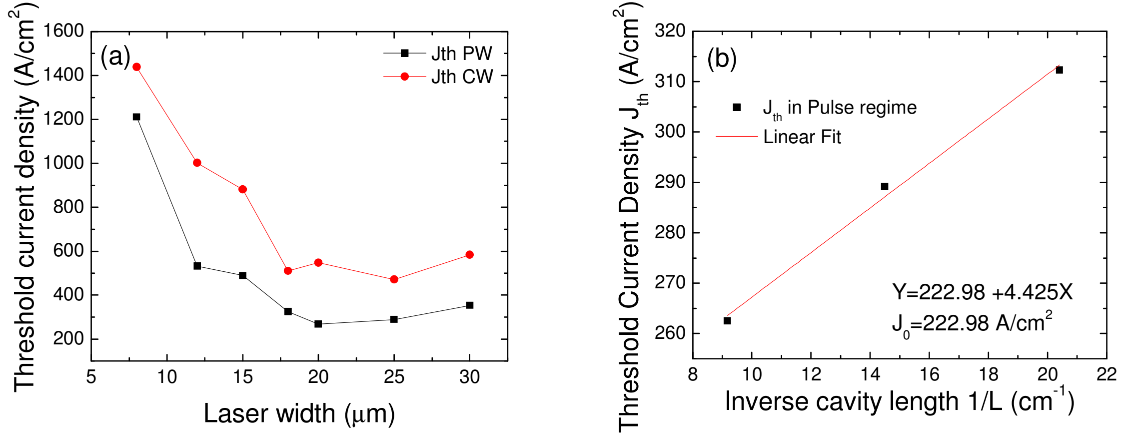

Figure 6: (a) Threshold current as a function of laser width (device length 690 µm) (b) Threshold current density as a function of inverse cavity length for a laser width of 25µm

Figure 6(a) shows the threshold current density as a function of laser mesa width (laser cavity length: 690µm). The increase of J_{th} at narrow widths indicates the increase in loss due to surface recombination, current leakage and scattering of the laser mode at the etched sidewalls. The threshold current density is plotted as a function of the inverse cavity length in figure 6(b) for pulsed operation. This results in a threshold current density of 223 A/cm^2 at infinite length. This result is relative high, which is probably due to non-optimum fabrication resulting in high loss.

4.2 Thermal characteristics

Figure 7(a) represents the LI characteristic as a function of temperature. By fitting the natural logarithm of J_{th} as a function of temperature as shown in figure 7(b), the T_0 parameter can be determined [14]. A T_0 of 44K is estimated. Alternatively, the thermal resistance R_{th} can also be used to assess the thermal characteristics of the laser [15]. The thermal resistance is defined as in equation (1)

$$R_{th} = \frac{\Delta T}{P_{therm}} = \left(\frac{\Delta\lambda}{\Delta T}\right)^{-1} . \frac{\Delta\lambda}{P_{therm}} \qquad [1]$$

where P_{therm} is the power consumption of the laser, ΔT is the temperature change of the active region and Δλ is the associated change in laser emission wavelength. Figure 8(a) represents the linear interpolation of wavelength drift as a function of temperature, when the laser is operated in pulsed regime, such that self-heating can be avoided. Figure 8(b) represents the wavelength drift as a function of power consumption. By using equation (1), the thermal resistance is estimated to be 323K/W. This high thermal impedance, compared to traditional laser fabrication [16] is related to the relatively thick adhesive bonding layer (660nm) used in these devices to optically isolate the laser mode from the substrate. Given the low thermal conductivity of the adhesive bonding layer (0.3W/mK) a high thermal impedance can be expected. Therefore, thermal management improvement is required. This is possible to implement by adding a thermal gold shunt [17] or by increasing the thickness of the gold contact.

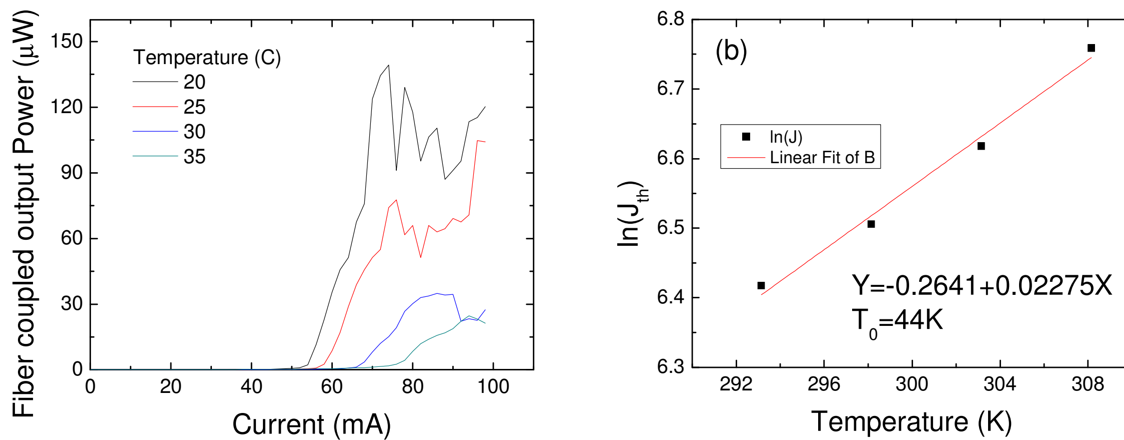

Figure 7: Temperature dependent characteristics of the thin-film lasers (18 µm wide and 490 µm long) (a) LI characteristic at different temperatures (b) Natural logarithm of J_{th} as a function of temperature to determine T_0

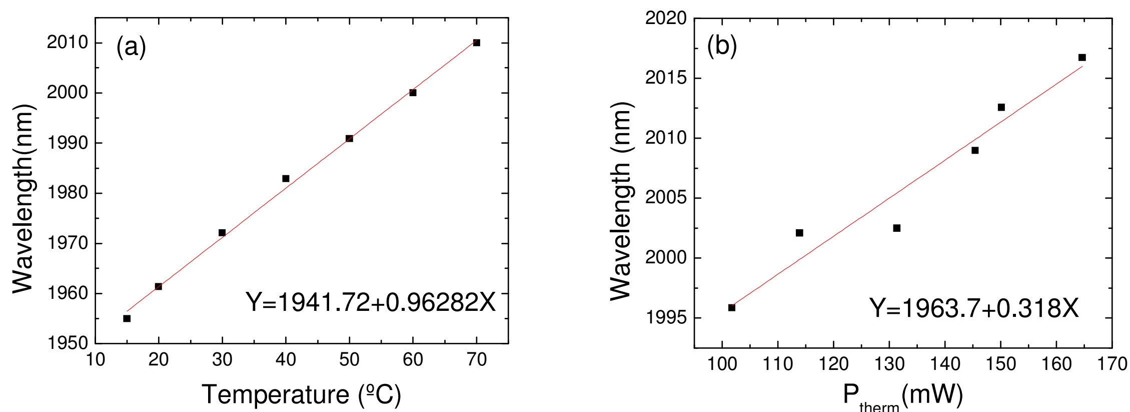

Figure 8: Lasing wavelength change as a function of a) carrier temperature (pulsed operation, so no self-heating) b) power consumption

4.3 Specific Contact Resistance

In order to improve current injection, assessment of the contact resistance is necessary. This is done using a transmission line model measurement technique [18]. The deposition of the P and N contact is performed immediately after the substrate removal and wet mesa etching process respectively. There is no surface treatment used. By plotting the resistance as a function of the distance between 100µm by 100µm contact pads, the specific contact resistance is determined. As shown in figure 9, the specific contact resistances of the p-contact and n contact are 4.5x10^{-4} Ohm.cm^2 and 20x10^{-4} Ohm.cm^2 respectively. These specific contact resistances are rather high due to the lack of surface treatment before metal deposition. Improvement is possible by using HCl or buffer HF before contact deposition [19].

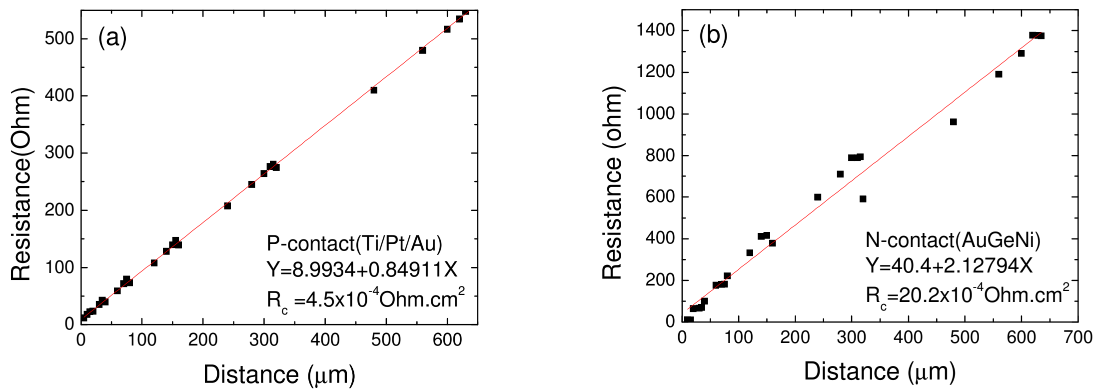

Figure 9: Resistance measured as a function of the distance between contact pads (a) P-contact (b) N-contact

5. CONCLUSION

In conclusion, we report for the first time integrated thin film GaSb FP lasers on an InP carrier. The devices operate at room temperature with low threshold current. While there is room for improvement in device performance, these results bring us significantly closer to fully integrated spectrometers on chip.

REFERENCES

[1] Miller, C. E., Brown L.R., " Near infrared spectroscopy of carbon dioxide I. ^{16}O ^{12}C ^{16}O line positions," J. Mol. Spectrosc., 228, 2, 329-354 (2004).

[2] Buchwitz, M., Rozanov. V. V., Burrows, J. P., "A near-infrared optimized DOAS method for the fast global retrival of atmospheric CH_4, CO, CO_2, H_2O and N_2O total column amounts from SCIAMACHY Envisat-1 nadir radiances," J. Geophys. Res., 105, No. D12, 15231-15245 (2000).

[3] Olesberg, J. T., Liu, L., Zee, V. V., Arnold, M. A., "In Vivo Near-Infrared Spectroscopy of Rat Skin Tissue with varying Blood Glucose Levels," Anal. Chem., 78, 215-223 (2006)

[4] Salhi, A., Barat, D., Romanini, D., Rouillard, Y., Ouvrard, A., Werner, R., Seufert, J., Koeth, J., Vicet, A., Garnache, A., "Single-frequency Sb-based distributed-feedback lasers emitting at 2.3 _m above room temperature for application in tunable diode laser absorption spectroscopy," Appl. Optics., 45, No. 20, 4957 - 4965 (2006).

[5] Ducanchez, A., Cerutti, L., Grech, P., Genty F., "Room-Temperature Continuous-Wave Operation of 2.3 µm Sb-Based Electrically Pumped Monolithic Vertical-Cavity Lasers," IEEE Photon. Technol. Lett., 20, No. 20, 1745-1747 (2008).

[6] N.A Yebo, W. Bogaerts, Z. Hens, R. Baets, "On-Chip Arrayed Waveguide Grating Interrogated Silicon-on-Insulator Microring Resonator Based Gas Sensor," IEEE Photon. Technol. Lett., 23(15), 1505-1507 (2011)

[7] http://www.epixfab.eu/

[8] N. Hattasan, B. Kuyken, F. Leo, E.M.P. Ryckeboer, D. Vermeulen, G. Roelkens, "High-efficiency SOI fiber-to-chip grating couplers and low-loss waveguides for the short-wave infrared," IEEE Photon. Technol. Lett., 24(17), 1536-1538 (2012).

[9] A. Gassenq, N. Hattasan, E.M.P. Ryckeboer, J.B. Rodriguez, L. Cerutti, E. Tournié, G. Roelkens, "Study of evanescently-coupled and grating-assisted GaInAsSb photodiodes integrated on a silicon photonic chip," Opt. Express, 20(11), 11665-11672 (2012).

[10] N. Hattasan, A. Gassenq, L. Cerutti, J. B. Rodriguez, E. Tournié, G. Roelkens, "Heterogeneous integration of GaInAsSb p-i-n photodiodes on a silicon-on-insulator waveguide circuit," IEEE Photon. Technol. Lett., 23, 1760 (2011).

[11] Fang, A. W., Cohen, O., Jones, R., Paniccia, M. J., Bowers, J. E., "Design and Fabrication of Optically Pumped Hybrid Silicon-AlGaInAs Evanescent Lasers," IEEE J. Sel. Topics Quantum Electron, 12, No.6, 1657-1663 (2006).

[12] Fang, A. W., Park, H., Cohen, O., Jones, R., Paniccia, M. J., Bowers, J. E., "Electrically pumped hybrid AlGaInAs-silicon evanescent laser," Opt. Express, 14, 9203-9210 (2006)
[13] http://camfr.sourceforge.net/
[14] Mobarhan, K. S., "Application note: Test and Characterization of Laser Diodes: Determination of Principal Parameters," < http://www.newport.com/servicesupport/PDF_Files/APPNOTE1.pdf> (19 November 2012)
[15] Leers, M., Boucke1, K.,Götz, M., Meyer, A., Kelemen, M., Lehmann, N., di Sopra, F. M., "Thermal resistance in dependence of diode laser packages," Proc. Of SPIE, 6876, 687609 (2008)
[16] Turner, G. W., Choi, H. K., Manfra, M. J., "Ultralow-threshold (50A/cm^2) strained single-quantum-well GaInAsSb/AlGaAsSb lasers emitting at 2.05 µm," Appl. Phys. Lett., 72, 876-878 (1998)
[17] Park. H., "Silicon Evanescent Devices for Optical Networks and Buffers," PhD Dissertation, 2008
[18] Reeves G. K., Harrison, H. B., "Obtaining the Specific Contact Resistance from Transmission Line Model Measurements," IEEE Electr. Device. L., EDL-3, No. 5, 111-113 (1982)
[19] Bijan, T., Carl S. K., Mohammad, F., Saied, T., Jeffrey A. M., "Extremely low specific contact resistivities for p-type GaSb, grown by molecular beam epitaxy," J. Vac. Sci. Technol. B, 13, 1, 1-3 (1995)